

# Structural Basis for the Mechanism of Ca<sup>2+</sup> Activation of the Di-Heme Cytochrome c Peroxidase from *Pseudomonas nautica* 617

João M. Dias,<sup>1</sup> Teresa Alves,<sup>1</sup> Cecília Bonifácio,<sup>1</sup>  
Alice S. Pereira,<sup>1</sup> José Trincão,<sup>1</sup>  
Dominique Bourgeois,<sup>2,3</sup> Isabel Moura,<sup>1</sup>  
and Maria João Romão<sup>1,\*</sup>

<sup>1</sup>REQUIMTE/CQFB

Departamento de Química, FCT  
Universidade Nova de Lisboa  
2829-516 Caparica  
Portugal

<sup>2</sup>LCCP, UMR 5075, IBS

41 avenue Jules Horowitz  
38027 Grenoble Cedex 1  
France

<sup>3</sup>ESRF

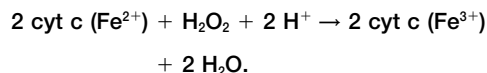
6 rue Jules Horowitz  
BP 220, 38043 Grenoble Cedex  
France

## Summary

Cytochrome c peroxidase (CCP) catalyses the reduction of H<sub>2</sub>O<sub>2</sub> to H<sub>2</sub>O, an important step in the cellular detoxification process. The crystal structure of the di-heme CCP from *Pseudomonas nautica* 617 was obtained in two different conformations in a redox state with the electron transfer heme reduced. Form IN, obtained at pH 4.0, does not contain Ca<sup>2+</sup> and was refined at 2.2 Å resolution. This inactive form presents a closed conformation where the peroxidatic heme adopts a six-ligand coordination, hindering the peroxidatic reaction from taking place. Form OUT is Ca<sup>2+</sup> dependent and was crystallized at pH 5.3 and refined at 2.4 Å resolution. This active form shows an open conformation, with release of the distal histidine (His71) ligand, providing peroxide access to the active site. This is the first time that the active and inactive states are reported for a di-heme peroxidase.

## Introduction

Cytochrome c peroxidases (CCPs) catalyze the two-electron reduction of hydrogen peroxide to water by one-electron donors such as cytochromes c or cup-redoxins, according to the reaction:



They are found in many different organisms from eukaryotes to prokaryotes, like plants, yeast, or bacteria. The most extensively studied bacterial CCPs are the ones isolated from *Pseudomonas* (*Ps.*) *aeruginosa* and *Paracoccus* (*Pa.*) *denitrificans* (Fülöp et al., 1995; Moura et al., 1999). Recently, a new bacterial CCP was purified from the marine denitrifier *Ps. nautica* 617. Under microaerophilic conditions, the cells of *Ps. nautica* 617 ex-

press the periplasmic enzyme CCP. This enzyme catalyzes the reduction of H<sub>2</sub>O<sub>2</sub> to H<sub>2</sub>O coupled to the oxidation of the monoheme cytochrome c<sub>552</sub>, which was identified as the physiological electron donor (Alves et al., 1999). This activity is a mechanism of protecting the cells from the toxicity of hydrogen peroxide (Halliwell and Gutteridge, 1984; Cheeseman and Slater, 1993). The enzyme is a homodimer of 2 × 36.5 kDa, corresponding to 326 amino acid residues. Sequence comparison showed that the *Ps. nautica* enzyme exhibits a high similarity with the homologous proteins from *Pa. denitrificans* (Goodhew et al., 1990; Pettigrew, 1991) and *Ps. aeruginosa* (Ellfolk and Soininen, 1970; Foote et al., 1983). Like other CCPs, this enzyme contains two heme c groups: a high-potential heme (HP) that functions as an electron transfer center located in the C-terminal domain and a low-potential heme (LP) that corresponds to the peroxidatic center located in the N-terminal domain (Fülöp et al., 1995; Shimizu et al., 2001). In the oxidized form of bacterial CCPs, a methionine and a histidine residue coordinate the HP heme iron atom, which is in equilibrium between high and low spin states. The LP heme is in the low-spin state and is coordinated by two histidine residues. In the oxidized form, the enzyme is inactive. The active form is obtained either by reduction with the physiological electron donor or non-physiologically by the addition of sodium ascorbate, both in the presence of calcium ions. This activation reaction results in the transition of the LP heme to a high-spin state with the loss of one of the histidine ligands, allowing substrate binding. The requirement of Ca<sup>2+</sup> ions for the activation of bacterial CCPs has also been observed in other nonbacterial enzymes, namely in the horseradish and lignin peroxidases (Gajhede et al., 1997; Poulos et al., 1993; Piontek et al., 1993).

Based on the different spectroscopic and electrochemical results obtained on *PadCCP*, two mechanisms have been proposed for the activation process (Prazeres et al., 1995; Lopes et al., 1998). In the first model, the electron transfer and peroxidatic hemes are the high- and low-potential heme, respectively. In the active form, the HP heme is in a low-spin state, while the LP heme loses its sixth histidine ligand, becoming high-spin. In the second model, there is a concomitant modification of the coordination sphere of both hemes; in the LP heme, His85 is replaced by Met129 while the HP heme loses its sixth methionine ligand.

In 1995, Fülöp and collaborators solved the crystal structure of the fully oxidized *PsaCCP* (Fülöp et al., 1995), and in 2001, the *Nitrosomonas* (*N.*) *europaea* structure was published (Shimizu et al., 2001). Despite the availability of these two crystal structures, it was not possible to distinguish between each of those models, as both could be explained in light of these structures. The structural data now reported seem to favor the first model for the activation process and present the first structure of a di-heme peroxidase in the active and inactive forms, allowing insight into the process of calcium activation and internal electron transfer pathway.

\*Correspondence: mromao@dq.fct.unl.pt

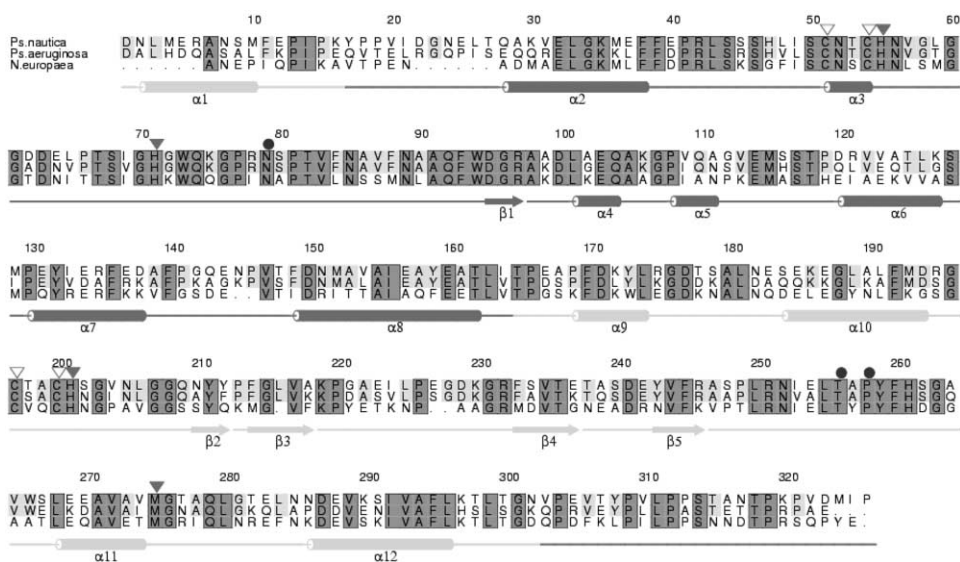


Figure 1. Multiple Sequence Alignment of the Cytochrome c Peroxidases for Which the Crystallographic Structure Is Determined *Ps. nautica* CCP (this work), *Ps. aeruginosa* CCP (Fülöp et al., 1995), *Nitrosomonas europaea* CCP (Shimizu et al., 2001). The secondary structure corresponds to form IN *PsnCCP* structure. Strand  $\beta 1$  and helix  $\alpha 4$  are not present in form OUT. The cysteine residues that covalently bind the two hemes are marked with a white triangle. The heme-iron ligands are marked with black triangles. The calcium protein ligands in form OUT are marked with a black circle. Figure prepared with ALSCRIPT (Barton, 1993)

## Results and Discussion

### Primary Sequence Analysis

The comparison of the full CCP sequences from *Ps. nautica* and *Ps. aeruginosa* reveals a sequence homology of 80% and 64% identity. The comparison between *PsnCCP* and *NieCCP* shows a lower homology of 73% with 49% identical amino acid residues. The multiple sequence alignment of the three sequences for which a crystallographic structure is known is represented in Figure 1.

### Characterization of the Crystals by Microspectrophotometry

*PsnCCP* was crystallized in two different forms obtained at pH 4.0 and pH 5.3, corresponding to form IN (inactive) and form OUT (active), respectively (Dias et al., 2002). In order to characterize the redox state of the native crystals, the absorption spectra of the crystals for both forms were acquired before and after X-ray exposure (Figure 2A). The high absorption by the crystals prevented the resolution of the Soret band maximum at 400 nm. Before X-ray exposure, the spectra of forms IN and OUT (Figure 2A, a and b) show that they are in the oxidized form, by comparison to the spectra of the native protein in solution, which is oxidized (Figure 2B, a) (Alves et al., 1999). After exposure to X-rays and full data collection at the ESRF, both crystal forms get reduced with the increase of the absorption of the  $\alpha$  and  $\beta$  bands (Figure 2A, c and d). Reduction of the crystals was also observed using Cu-K $\alpha$  radiation from an in-house rotating anode (data not shown). Attempts at crystal reduction with sodium ascorbate and sodium dithionite were unsuccessful, as no changes were observed in the oxidized spectra of the crystals, probably due to the low pH

(4.0 and 5.3) of the crystallization solutions. Experiments with protein in solution confirmed the difficulty in reducing the protein at these pH values. Unfortunately, the crystals are extremely fragile, and when they are transferred to a solution with a higher pH, they start degrading and reduction could not be achieved.

The phenomenon of radiation damage in protein crystals has been demonstrated in several cases where diffraction data were collected with synchrotron radiation (Weik, et al., 2000). The ability of X-rays to reduce protein crystals is particularly important in the case of redox enzymes (Karlsson et al., 2000). In 2002, this property was used for the first time in order to obtain different redox states of horseradish peroxidase and to study its catalytic pathway (Berglund et al., 2002).

### Overview of the Structures

The structural description is based on the form IN structure, as both structures present a similar fold. A stereoview of the overall structure is represented in Figure 3 for both crystal forms. The CCP polypeptide fold is of the  $\alpha/\beta$  type, consisting of 12  $\alpha$  helices and 5  $\beta$  strands. The topology of the molecule is organized into two domains, the LP and the HP domains. Each domain accommodates one heme center, and the hydrophobic interface between both domains harbors a calcium binding site, as observed in the other CCP structures (Fülöp et al., 1995, Shimizu et al., 2001). Both domains are formed by two noncontiguous stretches of the polypeptide chain. Domain LP is defined by residues 17–164 and 303–326 and binds the low potential heme, which presents as a heme binding motif: Cys51-X-Y-Cys54-His55...-His71-. This domain has a typical class 1 c type cytochrome (cyt) fold (Pettigrew and Moore, 1990). At the domain interface lays  $\beta 1$ , which interacts with  $\beta 5$  from

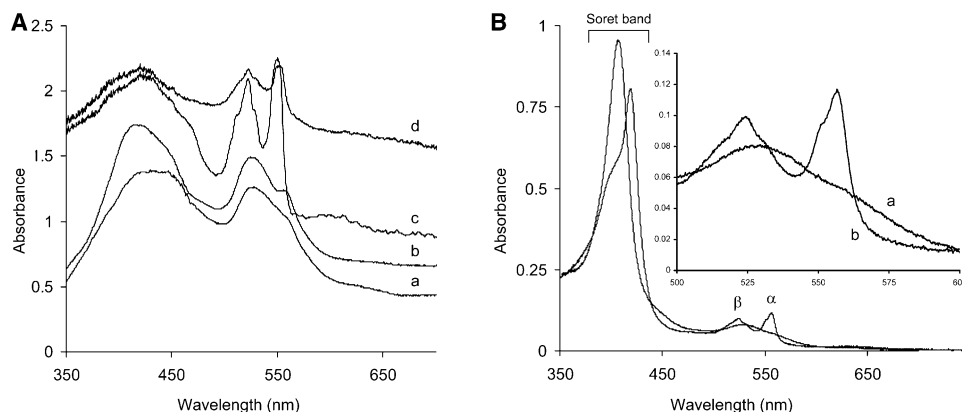


Figure 2. Optical Spectra of *Ps. nautica* CCP

(A) Optical spectra of *Ps. nautica* CCP cryocooled crystals (100 K). (a) Form IN (pH 4.0) crystals before X-ray exposure at ESRF; (b) form OUT (pH 5.3) crystals before X-ray exposure at ESRF; (c) form IN after X-ray exposure at ESRF; (d) form OUT after X-ray exposure at ESRF. (B) Optical spectra of *Ps. nautica* CCP in solution. (a) Native enzyme (oxidized); (b) sodium ascorbate reduced enzyme with 1 mM of  $\text{CaCl}_2$  added (semireduced).

domain HP. Domain HP consists of two noncontiguous polypeptides and comprises residues 1–16 and 165–302. The HP heme is covalently attached to residues Cys197 and Cys200 and exhibits the heme c binding motif: -Cys197-X-Y-Cys200-His201-...-Met275-. This domain also contains a typical class 1 c type cytochrome fold. The presence of the calcium binding site constrains the segment 256–258 and prevents the  $\alpha$  helical conformation. The HP heme separates this helical subdomain from the  $\beta$  features of the exterior of domain HP that contains four  $\beta$  strands.  $\beta$ 3 and  $\beta$ 4 form an antiparallel  $\beta$  sheet, which is covered at the top by another antiparallel  $\beta$  sheet formed by  $\beta$ 2,  $\beta$ 5, and also by the interaction of  $\beta$ 5 with  $\beta$ 1 from domain LP, at the domain interface.

The spatial arrangement of domains LP and HP creates a cavity at their interface, which accommodates the calcium binding site located 12 Å away from the LP heme Fe atom, 14 Å from the HP heme Fe and  $\sim$ 8 Å from the surface. A pseudo-2-fold axis runs across the molecule, which relates the HP heme and helices  $\alpha$ 10,  $\alpha$ 11, and  $\alpha$ 12 to the LP heme and helices  $\alpha$ 2,  $\alpha$ 5, and  $\alpha$ 8. A superposition of the cores of domain LP (106 out of 172 residues) and of domain HP (120 out of 154 residues) gives an rms deviation of 1.6 Å for 85 C $\alpha$  atoms, which reflects the structural similarity of both domains.

The comparison of forms IN and OUT by superposition of both structures (Figure 3C) shows that the larger differences are localized at the domain interface, in particular in the regions comprising loop 69–74 (including the distal His71), loop 96–108 (which lays at the domain interface and includes  $\beta$ 1), loop 276–283 near the HP heme, and the presence of the water/calcium, respectively.

#### Low-Potential Heme Domain

The enzyme was crystallized in its fully oxidized state, in form IN at pH 4.0, showing that the LP heme iron has two axial ligands, in agreement with spectroscopic data (Alves et al., 1999). Both ligands are histidines (His55 and His71). In type c cytochromes, a proline residue is positioned so that its carbonyl forms a hydrogen bond

with the N $\delta$  atom of the histidine coordinated to the heme iron, thus orienting the histidine ring. In CCP, His55 interacts in a similar way with Pro81 (3.17 Å) (Figure 4A). This histidine is also stabilized by a hydrogen bond with the carbonyl of Gly61 (3.22 Å). His71 is oriented preferentially through a hydrogen bond interaction with the carbonyl group of Glu114 (2.74 Å) (Figure 4A). For catalysis to take place, His71 must release from the LP heme iron to allow peroxide access. His71 belongs to a flexible loop (residues 68–78) on the accessible surface of the molecule, not far from the crystallographic dimer interface.

A different crystal form of the enzyme, form OUT, was crystallized at pH 5.3 and shows the presence of calcium. This result is consistent with protein activation, since His71 no longer coordinates the LP heme iron (Figure 4B), while the carbonyl of Gly61 moves to a distance of 3.50 Å, accompanying the slight movement of the loop which contains Asp62 and lies near the calcium binding pocket. His55 remains coordinating the heme, stabilized by the carbonyl interaction of Pro81 (2.97 Å). The LP heme is buried in the molecule and is covalently bound to cysteines 51 and 54. In form OUT, there is a salt bridge between the propionate A of the LP heme and NH1 of Arg246 (2.7 Å), and also a hydrogen bond to N $\delta$  of Asn89, while the other propionate (D) is stabilized by one hydrogen bond to the main chain nitrogen from Trp94 and by a water molecule. In form IN, the propionate A interacts with Arg246, Phe93, and Wat633, and the other propionate shows a conformational change and is stabilized by the NH1 of Arg78 and by Wat643.

#### High-Potential Heme Domain

The HP heme has His201 and Met275 as axial ligands to the heme iron. In both forms, the correct orientation of the histidine ring is maintained by the hydrogen bond between the N $\delta$  atom of His201 and the carbonyl of Ser248 (2.87 Å). The loop that comprises residues 223–228 is highly disordered and is not clear in the electron density, in both forms IN and OUT. Another short sol-

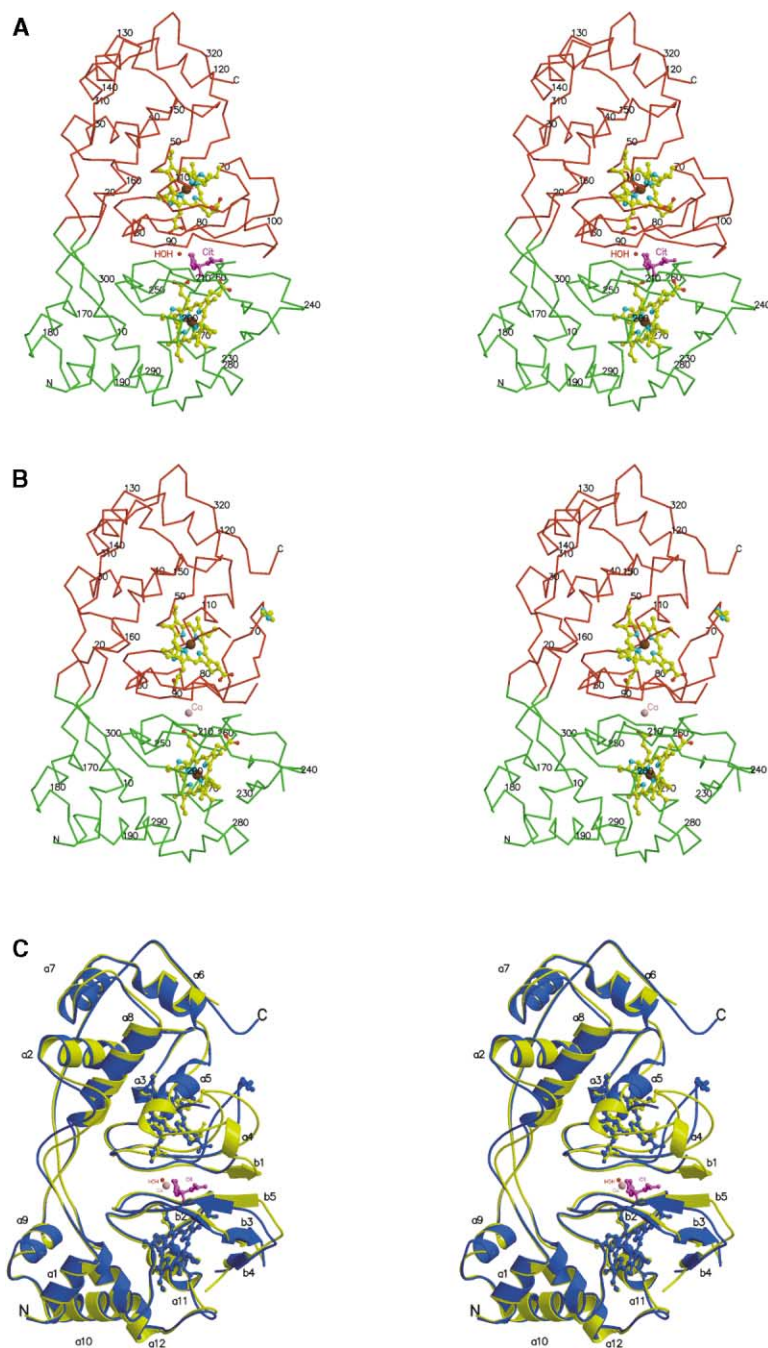


Figure 3. Stereo Representation of *Ps. nautica* CCP Structure

Domain LP, red; HP, green; hemes, yellow; calcium, pink; water, red.

(A) Form IN, inactive (pH 4.0).

(B) Form OUT, active (pH 5.3).

(C) Superposition of form IN (yellow) and form OUT (blue). Figures prepared with MOLSCRIPT (Kraulis, 1991) and RASTER-3D (Merritt and Bacon, 1997).

vent-exposed loop (276–282, also disordered in the structure of form OUT) shields the HP heme from the solvent.

In form OUT, there is a salt bridge between propionate D of the HP heme and the  $N\delta$  of His261, and a hydrogen bond between the main chain nitrogen from Leu216, while propionate A is stabilized by the hydrogen bonds to the main chain nitrogen N from Phe260 and to three water molecules.

In form IN, there is a salt bridge between propionate D of the HP heme and His261 and two hydrogen bonds, one with the main chain nitrogen from His261 and another with the main chain nitrogen from Leu216, while

propionate A is stabilized by hydrogen bonds to the main chain nitrogen from Phe260 and to a water molecule. Phe260 is placed in a highly hydrophobic region (Leu216, Phe233, Val235, Val265, Ala271, Val274, Tyr259, Met275, as well as HP heme). The propionate establishes several hydrogen bonds that impose stereochemical constraints in its vicinity. The tight interaction between the main chain and the propionate explains why Phe260 is a Ramachandran outlier.

#### Domain-Domain Interactions

The two domains are connected by three stretches of residues: residues 1–19, 160–169, and 296–326. The do-

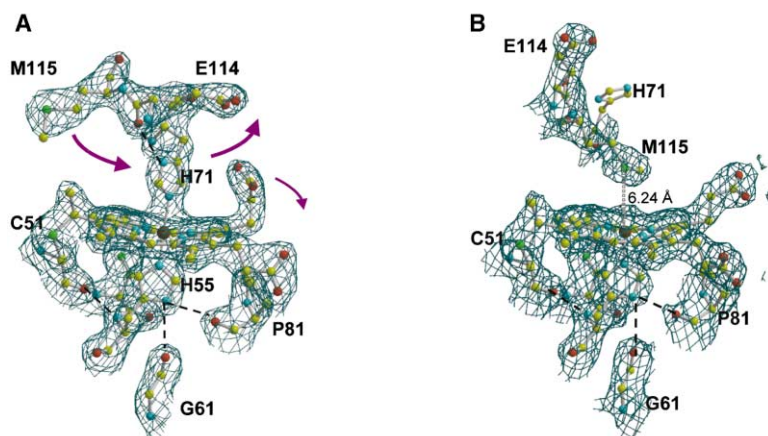


Figure 4. Simulated Annealing Omit Map around the Peroxidatic LP Heme and Surrounding Residues

(A) Form IN, inactive.  
(B) Form OUT, active. Figures prepared with TURBO-FRODO (Roussel and Cambillau, 1989).

main interactions are mainly hydrophobic, involving residues 60–66, 78–82, and 89–99 ( $\beta 1$ ) from LP domain and residues 204–213 ( $\beta 2$ ), 242–255–263 ( $\beta 5$ ) from HP domain. In form IN, the two domains interact through a network of hydrogen bonds, including  $\beta 1$  from the LP heme domain forming a three-stranded antiparallel  $\beta$  sheet with  $\beta 5$  and  $\beta 2$  from the HP heme domain.

In the cleft at the domain interface (Figure 5A), a citrate molecule from the crystallization buffer is present which contributes to the stabilization of the interdomain region through several hydrogen bonds with the main chain nitrogen from residues of both domains (Trp94, Arg246, Phe260) as well as with the side chain of Arg246. Three other citrate molecules were found in form IN. One of them is present in the N-terminal domain, near the LP heme, but does not contribute to the domain interaction, while two others are located in the solvent shell of the C-terminal domain.

In form OUT, the  $\beta$  sheet interaction is destabilized by the presence of the fully loaded calcium binding site between the two domains and the absence of a citrate molecule (Figure 5B). The disruption of strand  $\beta 1$  and of helix  $\alpha 4$  is observed, whose structure is no longer conserved. The main chain hydrogen bond Gly96 O-N Val244 is replaced by Gly96 N-O Val244, and there are 14 hydrogen bonds between both domains, 5 of which correspond to main chain hydrogen bonds.

#### Calcium Binding Site

In form OUT, the calcium binding site is fully occupied by a calcium ion ( $B_{\text{factor}} = 29.9 \text{ \AA}^2$  in comparison to an average of  $27.7 \text{ \AA}^2$  for neighboring atoms). This  $\text{Ca}^{2+}$  ion is coordinated by seven ligands in a distorted pentagonal bipyramidal geometry (Figure 5F): Asn79 O $\delta 1$  (2.41  $\text{\AA}$ ); Thr256 C=O (2.28  $\text{\AA}$ ); Pro258 C=O (2.44  $\text{\AA}$ ); and four water molecules ( $\sim 2.39 \text{ \AA}$ ). One of the propionates of the HP heme is hydrogen bonded to two of these water molecules (Wat502-HP heme O1A, 2.75  $\text{\AA}$ , and Wat504-HP heme O2A, 2.52  $\text{\AA}$ ). The calcium binding site imposes geometrical constraints that justify the preference for a *cis*-peptide conformation of Ala257-Pro258.

Despite the fact that form IN crystallized either in the presence or in the absence of  $\text{CaCl}_2$ , it was observed that the calcium binding site does not contain calcium,

which is replaced by a water molecule (Wat403) (Figure 5E). Attempts to refine this site as a calcium ion with full occupancy gave a  $B_{\text{factor}}$  of  $77.7 \text{ \AA}^2$  (while the neighboring atoms presented an average  $B_{\text{factor}}$  of  $42.0 \text{ \AA}^2$ ). Therefore, the site was refined as a water molecule with a  $B_{\text{factor}}$  of  $41.9 \text{ \AA}^2$  with surrounding atoms with an average  $B_{\text{factor}}$  of  $42.7 \text{ \AA}^2$ . Wat403 is within H bonding distance to O $\delta 2$  Asp62 (2.59  $\text{\AA}$ ), O=C Thr256 (2.23  $\text{\AA}$ ), O=C Pro258 (2.51  $\text{\AA}$ ), and to two water molecules (Wat632, 2.37  $\text{\AA}$ ; Wat698, 2.25  $\text{\AA}$ ). In the vicinity of this site, there is O $\delta 1$  Asn79 at 3.43  $\text{\AA}$  and O=C Ser80 at 3.83  $\text{\AA}$ .

The presence of the calcium ion introduces slight modifications in the surrounding atoms, with implications in the overall rearrangement of the internal hydrogen bond network. The distance between Asp62 and the calcium binding site increases from 2.47  $\text{\AA}$  (form IN, water) to 4.26  $\text{\AA}$  (form OUT, calcium). On the other hand, O $\delta 1$  of Asn79 moves in (3.72  $\text{\AA}$  to 2.44  $\text{\AA}$ ) and binds to the calcium ion.

One clear difference between forms IN and OUT is the disruption of some structural features near the calcium binding site, leading to protein movements, which may be correlated with the allosteric activation of the enzyme. Upon calcium binding, strand  $\beta 1$  and helix  $\alpha 4$  become disordered, while the movement of the loop containing the distal His71 pulls the helix  $\alpha 5$  away (Figure 3E). The calcium binding site may therefore modulate the interaction between the two domains, allowing conformational changes and allosteric regulation. The lack of compensating negative charges around the calcium ion suggests a functional role in modulating the electron transfer rates between the two heme domains, contributing to the fine-tuning of the heme redox potentials across the domain interface.

#### Electron Transfer Pathway

For the hydrogen peroxide reduction to take place at the LP peroxidatic heme, it is necessary that the electrons from the physiological partner cyt  $c_{552}$  be transferred first to the HP heme and then through an electron transfer pathway to the peroxidatic heme. The two heme groups are separated by an iron-iron distance of 21  $\text{\AA}$  and are positioned perpendicular to each other, such that one of the propionates of the HP heme points toward one propionate of the LP heme (Figures 5A and

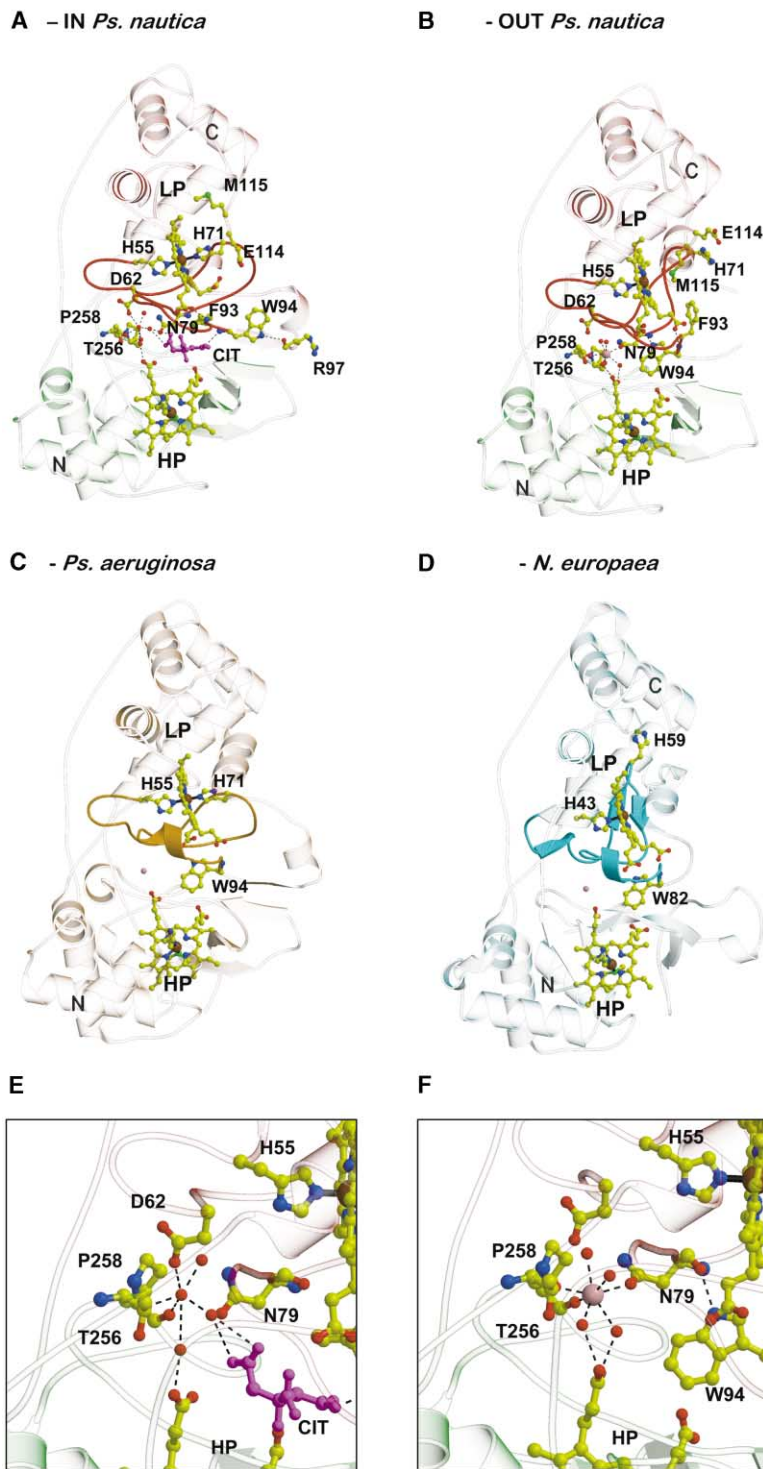


Figure 5. Structural Representation of CCPs: the Electron Transfer Pathway, Trp94 Conformational Switch Mechanism, and Calcium Binding Site

(A) Form IN, inactive.  
 (B) Form OUT, active.  
 (C) *Ps. aeruginosa* CCP.  
 (D) *N. europaea* CCP.  
 (E) Zoom of form IN showing the empty calcium binding site replaced by Water 403 (citrate in magenta).  
 (F) Zoom of form OUT calcium binding site. Calcium in pink. Figures prepared with MOLSCRIPT (Kraulis, 1991) and RASTER-3D (Merritt and Bacon, 1997).

5B). The shortest distance between the two hemes via these propionates is  $\sim 10$  Å, measured between the carboxylate groups (O2D401-O1D402), while the closest iron-iron distance between symmetry-related monomers in the physiological dimer is 27 Å.

The most likely electron transfer pathway between the two hemes is via the two heme propionates and involving the conserved Trp94, which lies in the same

plane as the HP heme and perpendicular to the LP heme. Comparing both crystal forms, in the active form OUT (Figure 5B), both Phe93 and Trp94 go through a conformational change, with Phe93 moving out of the pathway and enabling Trp94 to occupy the position blocked by the citrate molecule in form IN, between both heme propionates. This conformational change, simultaneously with the propionate conformational change, pro-

vides a favorable electron transfer pathway. The peptide nitrogen of Trp94 is within hydrogen bonding distance of the propionate of the LP heme (Trp94 N-O $\delta$ 2 LP heme, 2.73 Å). This mechanism of interaction may act as a conformational switch induced by the calcium activation and associated with the redox transitions in both hemes.

In the inactive form IN (Figure 5A), Trp94 adopts a conformation deviated away from the electron transfer pathway. Phe93 lies between both heme propionates, and a citrate molecule is placed at an intermediate position between the two hemes. The citrate molecule is only observed in form IN, although its presence in the crystallization solution is necessary for producing suitable crystals in both forms. In form IN, the concentration of citrate is much higher (0.8 M) than in form OUT (0.1 M).

Residue Trp94 and residues nearby (Q<sup>92</sup>FWDGR<sup>97</sup>) are conserved not only in the CCP family (Figure 1) but also among the mitochondrial cytochromes c (e.g., Trp59 in tuna cyt c) and in most class 1 cyt c. For example, in the crystal structure of the yeast cyt c-cyt c peroxidase complex, the electron transfer pathway requires the direct involvement of Trp191 (Pelletier and Kraut, 1992; Beratan et al., 1992). Recent electron transfer studies in protein crystals of zinc-substituted tuna cyt c (Tezcan et al., 2001) show that van der Waals interactions and water-mediated hydrogen bonds provide effective coupling elements for tunneling across protein-protein interfaces in protein crystals. The basis for the electron-tunneling theory comes from the works of Marcus and Sutin (1985), Tollin et al. (1986), and Beratan et al. (1992). These studies provide the theory that underlies the electron transfer phenomena in the photosynthesis and respiration processes, which commonly occur between protein-bound prosthetic groups that are separated by large molecular distances, often greater than 10 Å (Page et al., 1999; Mayo et al., 1986; Beratan et al., 1992; Moser et al., 1992; Balabin and Onuchic, 2000).

#### Mechanism of Calcium Activation and the Tryptophan Switch Model

In the inactive form IN, Trp94 presents a conformation that does not allow electron transfer between the two hemes (Figure 5A). This conformation is stabilized by the interaction of N $\epsilon$ 1 from Trp94 with the C=O of Arg97, and N-H Trp94 with C=O of Gln92 and O4 of citrate. In the active form OUT, the presence of the calcium ion promotes a rearrangement of the nearby residues, with implications in the hydrogen bond network, which stabilizes the Trp94 conformation. In this form, the interaction between Wat403 and Asp62 is replaced by the interaction of calcium with water molecule Wat505. At the same time, the O $\delta$ 1 from Asn79 moves in and binds to the calcium ion (Figure 5F). This provides the correct orientation of the carbonyl from Asn79, establishing the hydrogen bond with the N $\epsilon$ 1 of Trp94. This interaction stabilizes the conformational change of Trp94, placing this residue in the correct orientation for the electron transfer to occur. Simultaneously, the nitrogen from the Trp94 main chain interacts with the O2D of propionate D from the LP heme, and stabilizes its conformation in an "active" position, closing the circuit of the electron transfer between the two hemes (Figure 5B). Despite

the fact that Asp62 stays essentially in the same place, in the presence of calcium, the adjacent Asp63 changes its rotamer, with the reorientation of the main chain, which is reflected by the change of the Ramachandran position from a  $\beta$  region to an  $\alpha$ -helical conformation. The fact that Asp62 is not coordinating calcium enables the Asp63 carboxylate to interact with Ser80 in the active form. These interactions provide the fixation points for the flexibility of the whole segment that comprises residues 61–80. In the absence of calcium, the Trp94 interaction with Asn79 and the propionate D is lost, and both the Trp94 and the propionate adopt a conformation corresponding to the inactive form IN (Figure 5A).

The presence of high concentrations of citrate might pose a problem due to its presence in the interdomain region, but it cannot be argued that citrate has chelated calcium ions, because these were not present in form IN. On the other hand, it could be argued that the movement of Trp94 was due to displacement by the citrate molecule, since in the *Ps. aeruginosa* structure (also inactive form) (Figure 5C) the same Trp is not displaced. However, the *Ps. nautica* structure now reported is the only one obtained in the absence of added calcium ions, and therefore, the conformational switch involving Trp94 seems to be functional and correlated to the absence (inactive form) or presence (active form) of calcium.

#### Dimer Interactions

The dimer is stabilized by hydrophobic interactions between both C-terminal coiled coils of the two monomers. In addition, there are hydrophobic interactions among residues 39–66 including helix  $\alpha$ 3 and the C-terminal residues 303–326 from LP domain and residues 255–258 and 266 from domain HP. In form OUT, due to the His71 loop movement, the Trp73 stacks against its symmetry mate (Figure 6B).

The presence of calcium triggers conformational changes, which contribute to stronger interactions within the dimer. The nonaccessible surface area of the dimer in form OUT (3031 Å<sup>2</sup>) is higher than in form IN (2412 Å<sup>2</sup>), supporting the tighter interaction in the active form OUT (Figure 6).

The second calcium binding site suggested in the literature (Gilmour et al., 1995; Prazeres et al., 1995; Lopes et al., 1998; Moura et al., 1999) to be responsible for dimerization was not found in any of the crystal forms.

#### Proposed Catalytic Reaction Mechanism

Based on the different spectroscopic and electrochemical results obtained for *PadCCP*, two mechanisms have been proposed for the activation process (Prazeres et al., 1995; Lopes et al., 1998). In the first model (Figure 7), the electron transfer and peroxidatic hemes are the high- and low-potential heme, respectively. In the mixed-valence form, the active form, the HP heme is in a low-spin state and the LP heme loses its sixth histidine ligand, thus becoming high-spin. In the second model, the reduction of the HP heme is associated with the concomitant modification of the coordination sphere of both hemes: in the LP heme, His85 (His71 in *Ps. nautica*) is replaced by Met129 (Met115 in *Ps. nautica*), while the

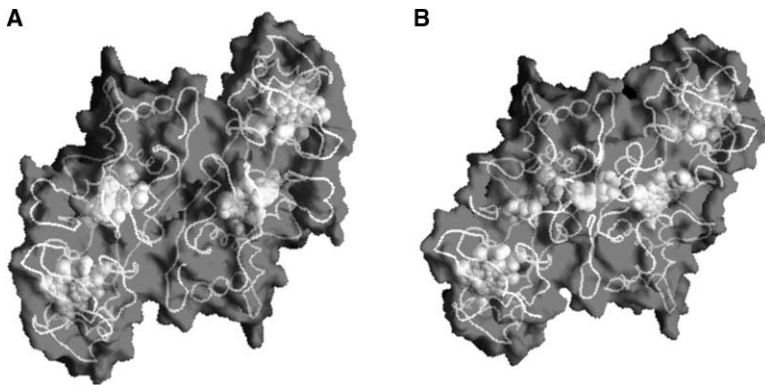


Figure 6. The CCP Homodimer  
(A) Form IN.  
(B) Form OUT shows the Trp73 stacking against its symmetry mate. Figures prepared with GRASP (Nicholls et al., 1991).

HP heme loses its sixth methionine ligand. Thus, in this model, there is a switching of the “spatial location” of the peroxidatic and electron transfer heme, ending up with the first one in the C-terminal part of the protein. Based on the available crystal structures, it is possible to suggest a reaction mechanism in agreement with model 1 (Figure 7). Domain HP accommodates the electron transfer heme and is supposed to mediate the electron transfer from cytochrome  $c_{552}$  to this heme group, which then transfers the electrons to the peroxidatic heme in the LP domain. The distal position of the peroxidatic heme becomes vacant during the peroxidatic reaction, and Met115 approaches the heme. In other peroxi-

dases, like horseradish peroxidase, the distal histidine and arginine residue (Arg38) could promote the acid-base catalysis and the heterolytic cleavage of the peroxide O-O bond in the compound I formation (Poulos and Kraut, 1980; Smith and Veitch, 1998; English and Tsaprailis, 1995). But an analogy to the di-heme *PsnCCP* is quite improbable, due to the drastic movement of 11 Å by the N $\epsilon$  of His71, which places this residue in a position too far away for its participation to take place. When the protein switches from form IN to form OUT, Met115 approaches the Fe atom from 10 to 6 Å but does not replace the distal histidine. In fact, mutagenesis studies in *Rhodobacter capsulatus* CCP of the corresponding

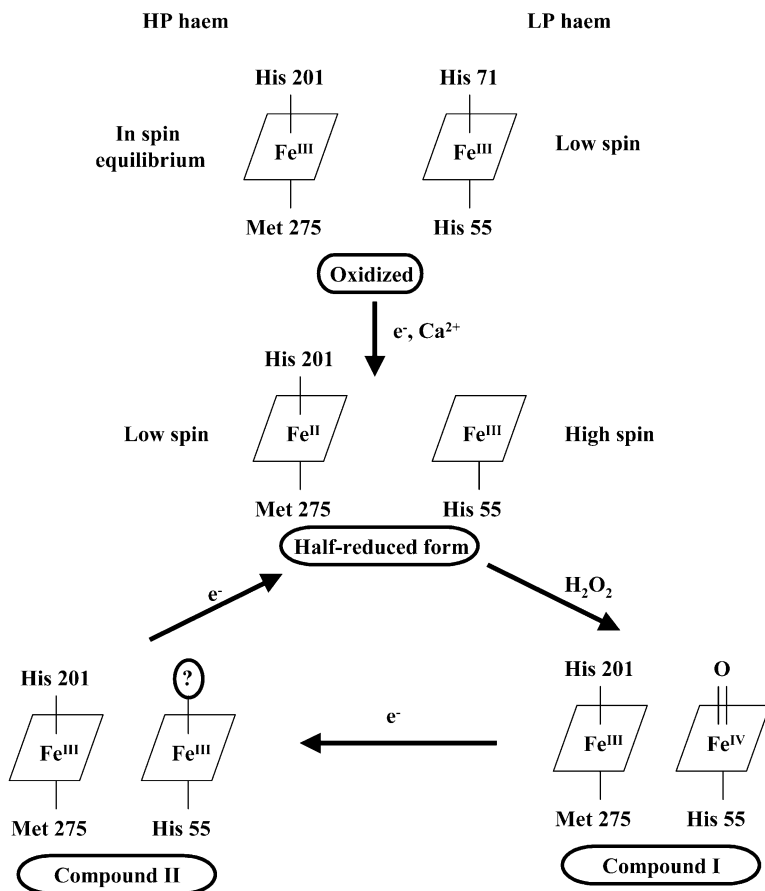


Figure 7. Proposed Reaction Mechanism Scheme  
(Adapted from Fülöp et al., 1995).

methionine to leucine show a  $\sim 10$ -fold decrease in the enzymatic activity (Smet et al., 2001). On the other hand, the coordination sphere of the HP heme does not change between the active and inactive forms, while the LP heme in the active form is five coordinated. Therefore, our structural data seem to favor model 1 for the activation mechanism.

Glu114, which lies in the active site pocket, could also play a role in enzymatic catalysis by acting as an acid-base catalyst promoting the heterolytic cleavage of the peroxide O-O bond in a similar way as suggested for the role of Glu102 for *NieCCP* by Shimizu et al. (2001). However, in form OUT the conformational orientation of Glu114 is not favorable, as it is pointing in the opposite direction of the LP heme, with 12 Å separating the nearest carboxylate from the Fe of LP heme.

### Relationship to Other Proteins

A structural search of *PsnCCP* with DALI (Holm and Sander, 1993) reveals, as expected, a very high structural homology with *PsaCCP* (Fülöp et al., 1995) (Figure 5C) and *NieCCP* (Shimizu et al., 2001) (Figure 5D). The Z score for the C $\alpha$  alignment of *PsnCCP* with *PsaCCP* is 40.2, which corresponds to a rmsd of 1.4 Å, considering 308 out of 326 amino acid residues, and the Z score for the alignment of *PsnCCP* with *NieCCP* is 31.3, which corresponds to a rmsd of 2.1 Å, considering 275 out of 326 amino acid residues.

Form OUT presents a conformation similar to *NieCCP*. The first helix  $\alpha 1$  is not present in *NieCCP*, but the overall fold is quite similar, with the exception of small displacements in specific loops and some amino acid residue insertions. In both structures, the loop 69–74, containing the distal histidine (His71 in *PsnCCP*, and His59 and the loop 57–62 in *NieCCP*), presents an open conformation. The hydrophobic interaction between the two monomers, which generates the physiological dimer, shares the Trp73 (Trp61 in *NieCCP*) stacking motif at the interface of the two monomers, as well as the hydrophobic interactions between the C-terminal loop. The electron transfer pathway is conserved through Trp94 (Trp 82 in *NieCCP*), and the heme propionates are placed in a similar orientation in both structures, which suggests that the *NieCCP* was obtained in the active form of the enzyme. The main differences reside in the fact that Met115 (Met103 in *NieCCP*) is placed closer to the heme pocket. Its side chain is placed in the same position as the Glu102 side chain of *NieCCP*, which was proposed to have a catalytic role in the heterolytic cleavage of the peroxide O-O bond (Shimizu et al., 2001). But further experimental evidence is needed in order to support methionine involvement in the catalytic reaction.

### Conclusions

The CCP from *Pseudomonas nautica* belongs to a group of peroxidases that require calcium activation correlated with a spin state transition of the peroxidatic heme.

Two crystal structures were obtained at different pH values. Both structures correspond to a redox state with the ET heme reduced as a result of the X-ray exposure. Form IN, obtained at pH 4.0, shows a closed conformation where the peroxidatic heme adopts a six-ligand

coordination, hindering the peroxidatic reaction from taking place. Form IN corresponds to the inactive form of the enzyme, with the calcium ion replaced by a water molecule at the calcium binding site. The structure is particularly ordered (the only disordered loop comprises residues 219–232) and resembles an inactive, oxidized state, structurally homologous to the *PsaCCP*. Form OUT, obtained at pH 5.3, shows an open conformation, due to the leaving of the distal histidine ligand (His71), providing peroxide access to the active site. This active form is achieved by binding of Ca $^{2+}$  ion and enzyme reduction, which is essential for enzymatic activation and is coupled to several conformational changes. The form OUT structure contains several disordered regions (loop 69–74 near the LP heme, region 97–115, loop 219–232, and loop 276–283 near the HP heme), which could reflect some intrinsic disorder of this crystal form. The presence of calcium enables allosteric activation and the consequent transition between structures IN and OUT, reflected by the large movement of the His71 loop, with direct implications in the low potential heme coordination.

In form OUT, the movement of loop 68–73 sets the peroxidatic heme free and allows for the reaction to occur, enabling the peroxidatic heme activation. Concomitantly, the simultaneous conformational change of the Trp94 and of the propionate of the peroxidatic heme, induced by the presence of Ca $^{2+}$ , facilitates electron transfer between the two hemes. The regeneration of the enzymatic activity is allowed by the flow of electrons from the physiological electron donor c552 to the HP heme, which finally directs the electrons to the peroxidatic heme, where the peroxide reduction to water takes place.

This study provides the first structural information on a CCP from the same organism obtained in two different catalytic forms, an inactive form obtained from an enzyme preparation without calcium and an active form obtained in the presence of calcium.

### Experimental Procedures

#### Protein Purification and Characterization

Cytochrome c peroxidase was purified from *Pseudomonas nautica* strain 617 (Pasteur Institute Collection, ref. *Ps. nautica* 617/1.85) (Bonin et al., 1987) in a four-step purification protocol, as described by Alves et al. (1999).

#### Gene Sequencing

*Ps. nautica* cells were grown as previously described (Alves et al., 1999). Genomic DNA was isolated using a standard CTAB extraction protocol (Reichardt and Rogers, 1998). The full CCP-encoding gene was amplified using two approaches. In the first approach, two classic PCR reactions were performed using degenerated primers. For the first reaction (PCR1), the primers were designed based on the N terminus of the protein (5'-CTC[G]GGCAAGATGGAG[A]TTC-3' as the forward primer) and on amino acid sequence homologies with other bacterial CCP (5'-GGAAG[A]TAC[G]GGG[C]GCG[C]G-3' as the reverse primer). To gain information on the C-terminal region, a second PCR reaction (PCR2) was done in which the forward primer was homologous to the N terminus (5'-GACAACTG[C]ATGGA G[A]CG-3') and the reverse primer was designed based on the amino acid sequence determined from the crystallographic electron density maps (5'-AGG[C]GTT[C]TTC[G]AGG[A]AAG[C]GC-3').

In both reactions,  $\sim 200$  ng of genomic DNA, 50 pmol of each primer, 0.2 mM of each dNTP, and 2.5 units of *taq* DNA polymerase

Table 1. Crystallographic Data and Data Collection Statistics from *Ps. nautica* CCP

Label	Form IN	Form OUT
pH of the crystal form	4.0	5.3
X-ray source	ID14-2, ESRF	ID14-1, ESRF
Wavelength (Å)	0.933	0.934
Crystal Data		
Space group	P3 <sub>1</sub> 21	P6 <sub>3</sub> 22
Unit cell parameters (Å)	a = b = 114.3, c = 90.5	a = b = 150.4, c = 155.3
V <sub>m</sub> /solvent content (%)	4.68/73.5	7.02/82.4
Mosaicity	0.32	0.27
Data Collection		
Resolution (Å)	25.0–2.20	30.0–2.40
Last resolution shell (Å)	2.28–2.20	2.49–2.40
Number of observations	494,949	351,446
Number unique reflections	35,359	41,056
R <sub>merge</sub> (%)	3.8	8.1
Last resolution shell (%)	29.2	45.8
Completeness (%)	99.9	99.2
Last resolution shell (%)	100.0	97.2
I/sigma (I)	32.1	15.8
Last resolution shell	7.2	3.1

in 1× PCR buffer (Amersham Pharmacia Biotech) were used, in a total volume of 50 µl. The reaction was performed in a thermal cycler (Biometra) using the following program: 1 cycle at 94°C for 10 min, followed by 35 cycles of 0.5 min at 94°C, 1.5 min at 51°C for PCR1 and 48°C for PCR2, 2 min at 72°C, and a final extension step for 10 min at 72°C. The PCR products were analyzed by electrophoresis in 1% agarose gel in the presence of ethidium bromide using 1× TAE buffer. PCR1 resulted in the amplification of a DNA fragment with approximately 650 bp, which represented about 69% of the total amino acid sequence of the protein, while a fragment of 864 bp was produced on PCR2 (92% of the total amino acid sequence). At this point, a total of 249 amino acids were known, which represented 79% of the full amino acid sequence of *PsnCCP*.

These fragments were purified from contaminants by gel extraction using the QIAquick Gel Extraction Kit (QIAGEN) and subse-

quently ligated into the commercial pGEM-T Easy vector from Promega according to the manufacturer's instructions. The resulting DNA plasmids were transformed into *Epicurian Coli* XL1-Blue competent cells (Stratagene), which were plated on Luria Broth agar medium containing 100 µg/ml ampicillin, 100 µg/ml X-gal, and 0.5 mM IPTG, grown overnight at 37°C. Positive recombinant clones were screened by their color, grown overnight at 37°C in LB medium with 100 µg/ml ampicillin, and confirmed by restriction digestion analysis with EcoRI. Plasmidic DNA from single transformants was isolated and sequenced with an Amersham Pharmacia ALF Express II automated sequencer using standard protocols (Sambrook et al., 1989). For identification, the obtained sequences were translated and compared with other amino acid sequences of bacterial CCPs published in the literature.

The remaining 78 bp of the *PsnCCP* encoding gene were obtained

Table 2. Refinement Parameters and Statistics for the *Ps. nautica* CCP Model

Crystal	Form IN	Form OUT
pH condition	4.0	5.3
Resolution limits (Å)	20.00–2.20	30–2.40
Number of unique reflections used in refinement	33291	37494
R factor of the final model	17.9	18.6
Free R factor of a test set containing 5% of reflections randomly chosen	19.9	20.9
Standard deviation from target values in:		
Bond lengths (Å)	0.009	0.014
Bond angles (°)	1.45	1.61
Number of non-H protein atoms	2386	2429
Number of non-H cofactor atoms		
2 × (heme Fe)	86	86
Calcium	0	1
Number of solvent atoms		
Water	333	296
Citrate	52	0
Temperature factors (Å <sup>2</sup> )		
Average for all non-H atoms	46.0	36.5
Average for protein atoms	44.2	35.8
Average for cofactor atoms	33.3	27.9
Average for solvent molecules	59.3	44.3
Ramachandran plot		
Most favored regions	264 (88.6%)	255 (87.5%)
Additional allowed regions	26 (11.0%)	32 (12.5%)
Disallowed regions	1 (0.4%)	1 (0.4%)

applying the Universal GenomeWalker Kit (CLONTECH) according to the manufacturer's instructions. For this purpose, the gene-specific primers (GSP) used were designed based on the previously known DNA sequence. Both PCR reactions required were performed using, respectively, the following genes specific primers: 5'-TAACATC GAGTGACCGCGCCTATTT-3' as GSP<sub>1</sub>, and 5'-TGGAAGAAGCC GTTGGCGGTGATGGGTA-3' as the GSP<sub>2</sub>. The PCR conditions were the ones described on the protocol adjusting the annealing temperatures to 78°C and 73°C for the primary PCR. For the secondary PCR, the same annealing temperatures were used. All oligonucleotides primers used were synthesized by Amersham Pharmacia Biotech.

#### Crystallization

CCP was crystallized as previously reported (Dias et al., 2002). Crystals were grown at pH 5.3 and pH 4.0, corresponding to two different crystal forms, forms OUT and form IN, respectively. Crystals of form OUT belong to space group P6<sub>3</sub>22, with unit cell parameters  $a = b = 150.4 \text{ \AA}$  and  $c = 155.3 \text{ \AA}$ , and were obtained in the presence of 1.0 M ammonium di-hydrogen phosphate as precipitant and 0.1 M sodium citrate (pH 5.3) at 4°C. Crystals of form IN belong to space group P3<sub>1</sub>21, with cell constants  $a = b = 114.3 \text{ \AA}$  and  $c = 90.5 \text{ \AA}$ , and were obtained with 0.8 M sodium citrate (pH 4.0) at 4°C. Previous incubation of the protein with 1 mM CaCl<sub>2</sub> prior to crystallization is absolutely required in order to obtain crystals at pH 5.3 (form OUT), while at pH 4.0 crystals were obtained independently of the presence of CaCl<sub>2</sub>. Considering one molecule per asymmetric unit, crystals of form OUT have a solvent content of 82%, based on a  $V_M$  of 7.0 Å<sup>3</sup>/Da (Mathews, 1968), and crystals of form IN show a solvent content of 74%, based on a  $V_M$  of 4.7 Å<sup>3</sup>/Da. In the *PsaCCP*, the solvent content is also high (61%) (Fülöp et al., 1993, 1995).

#### Microspectrophotometry of the Crystals

In the microspectrophotometric experiments, the crystals used were thinner than those used for X-ray diffraction in order to minimize the optical density and to maximize the signal-to-noise ratio. The crystals were prepared and transferred to a cryoprotectant solution as for X-ray experiments and were mounted on cryoloops on a goniometer head and then maintained at 100 K by a nitrogen gas stream. Spectra from crystals exposed with synchrotron radiation (ESRF) were collected in a microspectrophotometer set-up (Bourgeois et al., 2002) using light from a deuterium light source (Oriol, Stratford, CT) focused onto the sample (focal spot ~50 μm) via an optical fiber. The unpolarized transmitted light was analyzed using a CCD spectrometer (Ocean Optics, Dunedin, FL) providing a 200–850 nm wavelength range. The spectra of the crystals before X-ray exposure were measured in-house by the same procedure, but using the commercial 4DX System Microspectrophotometer (Uppsala, Sweden) with a xenon lamp providing spectral measurements in the 350–800 nm range. The dark current corresponding to the electronic noise was measured, and the baseline correction was performed with the cryoprotectant solution.

#### Data Collection and Reduction

X-ray diffraction data for crystals of form OUT were collected using synchrotron radiation at the ESRF (Grenoble) at ID14-EH1. For crystal form IN, data were collected at beamline ID14-EH2. All data were processed with DENZO and SCALEPACK (Otwinowski and Minor, 1997), and a summary of the data collection and final processing statistics is shown in Table 1.

#### Phase Determination

The crystal structures of both forms of *PsnCCP* were determined by molecular replacement as previously described (Dias et al., 2002). The calculations were performed using the crystal structure of CCP from *Ps. aeruginosa* as a search model (kindly provided by V. Fülöp prior to PDB deposition, PDB code 1EB7 [Fülöp et al., 1995]), which was edited according to sequence homology. The amino acid sequence of *Ps. aeruginosa* CCP is 64% identical to that of *Ps. nautica* CCP, with 80% of homologous amino acid residues.

The structure of crystal form OUT was solved first and was subsequently used to solve the crystal form IN. The structure was solved by molecular replacement using EPMR (Kissinger et al., 1999), and the solution was confirmed with AMORE (Navazza and Saludjian,

1997). The correct solution clearly emerged as a top peak with a correlation coefficient of 0.45 and an  $R_{\text{factor}}$  of 0.51. Calculations were carried out using all reflections between 20–4.0 Å resolution, and the space group P6<sub>3</sub>22 was found to be the correct one. For crystal form IN, the refined model of form OUT was used as a search model, and the correct solution was easily found as a clear top peak presenting a C.C. of 0.48 and an  $R_{\text{factor}}$  of 0.48, confirming the space group P3<sub>1</sub>21 as the only one giving a correct solution.

#### Model Building and Crystallographic Refinement

The asymmetric unit contains one monomer, and the biological functional homodimer is generated by crystallographic symmetry. At beginning of the refinement, the complete primary sequence of *PsnCCP* was unknown, and the initial edited model from *Ps. aeruginosa* was used, and side chains were gradually modified according to the known *Ps. nautica* sequence and on the basis of the electron density shape. The PCR-derived partial amino acid sequences were fitted into the experimental electron density, and errors in the tentative X-ray sequence were gradually corrected. As the refinement of the structure proceeded, the sequence was totally determined, included in the structure, and refined. Intermediate models were refined by simulated annealing protocols using the program CNS (Brünger et al., 1998), and in order to overcome model bias, some cycles of ARP-WARP (CCP4, 1994) in MOLREP mode were performed, and the resulting maps were carefully analyzed. For form OUT, the crystallographic  $R_{\text{factor}}$  is 18.60 in the resolution range from 30.00 to 2.40 Å using 37,494 reflections. The free R value (Brünger, 1992) is 20.91, based on 1984 (5%) randomly selected reflections. Electron density maps were interpreted with the programs O (Jones et al., 1991) and TURBO-FRODO (Roussel and Cambillau, 1989). Analysis with PROCHECK (Laskowski et al., 1993) shows that of 255 nonglycine and nonproline residues, 87.1% are in the most favored regions of the Ramachandran plot and 12.5% are in the additional allowed regions. Only Phe260 is in a nonallowed region of the Ramachandran plot, but it is very well defined in the electron density, and the geometrical constraint that causes this outlier is probably due to the stabilization of one of the propionates of the HP heme by the main chain (see Discussion). There are three regions that are not very well defined in the electron density (98–104, 219–229, and 276–282). The zone defined by residues 98–104 shows a conformational change between form OUT and IN, whereby strand β1 and helix α4 are stretched and disrupted in form OUT. Residues 219–229 correspond to an external disordered loop. The region that comprises residues 276–282 lies in an adjacent region to the HP heme distal ligand, Met275, with the electron density suggesting possible alternate conformations within this loop. For form IN, the crystallographic  $R_{\text{factor}}$  is 17.95% in the resolution range from 25.00 to 2.20 Å using 33,172 reflections. The free R value is 20.95% based on 1768 (5%) randomly selected reflections. Analysis with PROCHECK indicates that of the 264 nonglycine and nonproline residues, 89.6% fall in the most favored regions of the Ramachandran plot, with 10.0% in additional allowed regions, no residues in generously allowed regions, and only Phe260 in a nonallowed region, as in form OUT. The external loop that comprises residues 219–229 is not defined in the electron density. Crystal refinement data are summarized in Table 2.

Surface areas were calculated with SURFACE (Lee and Richards, 1971) from the CCP4 package (CCP4, 1994).

#### Acknowledgments

This work was supported by Ph.D grants PRAXIS XXI/BD/13530/97 and PRAXIS XXI/BD/18295/98 and POCTI grant SFRH/BPD/7136/2001, as well as by POCTI/42309/QUI/2001. We acknowledge Carlos Frazão for help and assistance with the 4DX Systems Microspectrophotometer at ITQB, Oeiras, and the EMBL Grenoble Outstation support for measurements at the ESRF under the European Union TMR/LSF Program.

Received: January 12, 2004

Revised: March 15, 2004

Accepted: March 19, 2004

Published: June 8, 2004

## References

- Alves, T., Besson, S., Duarte, L.C., Pettigrew, G.W., Girio, F.M.F., Devreese, B., Vandenberghe, I., Beeumen, J.V., Fauque, G., and Moura, I. (1999). A cytochrome *c* peroxidase from *Pseudomonas nautica* 617 active at high ionic strength: expression, purification and characterization. *Biochim. Biophys. Acta* 1434, 248–259.
- Balabin, I.A., and Onuchic, J.N. (2000). Dynamically controlled protein tunneling paths in photosynthetic reaction centers. *Science* 290, 114–117.
- Barton, G.J. (1993). ALSCRIPT, a tool to format multiple sequence alignments. *Protein Eng.* 6, 37–40.
- Beratan, D.N., Onuchic, J.N., Winkler, J.R., and Gray, H.B. (1992). Electron-tunneling pathways in proteins. *Science* 258, 1740–1741.
- Berglund, G.I., Carlsson, G.H., Smith, A.T., Szöke, H., Henriksen, A., and Hajdu, J. (2002). The catalytic pathway of horseradish peroxidase at high resolution. *Nature* 417, 463–468.
- Bonin, P., Gilewicz, M., and Bertrand, J.C. (1987). Denitrification by a marine bacterium *Pseudomonas nautica* strain 617. *Ann. Inst. Pasteur Microbiol.* 138, 371–383.
- Bourgeois, D., Vernede, X., Adaqm, V., Fioravanti, E., and Ursby, T. (2002). A novel microspectrophotometer for absorption and fluorescence studies of protein crystals. *J. Appl. Crystallogr.* 35, 319–326.
- Brünger, A.T. (1992). The free R value: a novel statistical quantity for assessing the accuracy of crystal structures. *Nature* 355, 472–474.
- Brünger, A.T., Adams, P.D., Clore, G.M., DeLano, W.L., Gros, P., Grosse-Kunstleve, R.W., Jiang, J.S., Kuszewski, J., Nilges, M., Pannu, N.S., et al. (1998). Crystallography and NMR system: a new software suite for macromolecular structure determination. *Acta Crystallogr. D* 54, 905–921.
- CCP4 (Collaborative Computational Project 4) (1994). The CCP Suite: programs for protein crystallography. *Acta Crystallogr. D* 50, 760–763.
- Cheeseman, K.H., and Slater, T.F. (1993). An introduction to free radical biochemistry. *Br. Med. Bull.* 49, 481–493.
- Dias, J.M., Bonifácio, C., Alves, T., Moura, J.J.G., Moura, I., and Romão, M.J. (2002). Crystallization and preliminary X-ray diffraction analysis of two pH-dependent forms of a di-heme cytochrome *c* peroxidase from *Pseudomonas nautica*. *Acta Crystallogr. D* 58, 697–699.
- Ellfolk, N., and Soininen, R. (1970). *Pseudomonas* cytochrome *c* peroxidase. I. Purification procedure. *Acta Chem. Scand. A* 24, 2126–2136.
- English, A.M., and Tsapralis, G. (1995). Catalytic structure-function relationships in heme peroxidases. *Adv. Inorg. Chem.* 43, 79–125.
- Foote, N., Thompson, A.C., Barber, D., and Greenwood, C. (1983). *Pseudomonas* cytochrome C-551 peroxidase. A purification procedure and study of CO-binding kinetics. *Biochem. J.* 209, 701–707.
- Fülöp, V., Little, R., Thompson, A., Greenwood, C., and Hajdu, J. (1993). Crystallization and preliminary x-ray analysis of the di-heme cytochrome *c* peroxidase from *Pseudomonas aeruginosa*. *J. Mol. Biol.* 232, 1208–1210.
- Fülöp, V., Ridout, C.J., Greenwood, C., and Hajdu, J. (1995). Crystal structure of the di-heme cytochrome *c* peroxidase from *Pseudomonas aeruginosa*. *Structure* 3, 1225–1233.
- Gajhede, M., Schuller, D.J., Henriksen, A., Smith, A.T., and Poulos, T.L. (1997). Crystal structure of horseradish peroxidase *c* at 2.15 Å resolution. *Nat. Struct. Biol.* 4, 1032–1038.
- Gilmour, R., Prazeres, S., McGinnity, D.F., Goodhew, C.F., Moura, J.J.G., Moura, I., and Pettigrew, G.W. (1995). The affinity and specificity of Ca(2+)-binding sites of cytochrome-*c* peroxidase from *Paracoccus denitrificans*. *Eur. J. Biochem.* 234, 878–886.
- Goodhew, C.F., Wilson, I.B.H., Hunter, D.J.B., and Pettigrew, G.W. (1990). The cellular location and specificity of bacterial cytochrome *c* peroxidases. *Biochem. J.* 271, 707–712.
- Halliwell, B., and Gutteridge, J. (1984). Oxygen toxicity, oxygen radicals, transition metals and disease. *Biochem. J.* 219, 1–14.
- Holm, L., and Sander, C. (1993). Protein structure comparison by alignment of distance matrices. *J. Mol. Biol.* 233, 123–138.
- Jones, T.A., Zou, J.Y., Cowan, S.J., and Kjeldgaard, M. (1991). Improved methods for binding protein models in electron density maps and the location of errors in these models. *Acta Crystallogr. A* 47, 110–119.
- Karlsson, A., Parales, J.V., Parales, R.E., Gibson, D.T., Eklund, H., and Ramaswamy, S.J. (2000). The reduction of the Rieske iron-sulfur cluster in naphthalene dioxygenase by X-rays. *J. Inorg. Biochem.* 78, 83–87.
- Kissinger, C.R., Gehlhaar, D.K., and Fogel, D.B. (1999). Rapid automated molecular replacement by evolutionary search. *Acta Crystallogr. D* 55, 484–491.
- Kraulis, P.J. (1991). MOLSCRIPT: a program to produce both detailed and schematic plots for protein structures. *J. Appl. Crystallogr.* 24, 946–950.
- Laskowski, R.A., McArthur, M.W., Moss, D.S., and Thornton, J.M. (1993). PROCHECK—a program to check stereochemical quality of protein structures. *J. Appl. Crystallogr.* 26, 283–291.
- Lee, B., and Richards, F.M. (1971). The interpretation of protein structures: estimation of static accessibility. *J. Mol. Biol.* 55, 379–400.
- Lopes, H., Pettigrew, G.W., Moura, I., and Moura, J.J.G. (1998). Electrochemical study on cytochrome *c* peroxidase from *Paracoccus denitrificans*: a shifting pattern of structural and thermodynamic properties as the enzyme is activated. *J. Biol. Inorg. Chem.* 3, 632–642.
- Marcus, R.A., and Sutin, N. (1985). Electron transfers in chemistry and biology. *Biochim. Biophys. Acta* 811, 265–322.
- Mathews, B.W. (1968). Solvent contents of protein crystals. *J. Mol. Biol.* 33, 491–497.
- Mayo, S.L., Ellis, W.R., Crutchley, R.J., and Gray, H.B. (1986). Long-range electron transfer in heme proteins. *Science* 233, 948–952.
- Merritt, E.A., and Bacon, D.J. (1997). Raster3D. Photorealistic molecular graphics. *Methods Enzymol.* 277, 505–524.
- Moser, C.C., Keske, J.M., Warncke, K., Farid, R.S., and Dutton, P.L. (1992). Nature of biological electron transfer. *Nature* 355, 796–802.
- Moura, I., Lopes, H., Costa, C., Moura, J.J.G., and Pettigrew, G.W. (1999). Spectroscopic studies on di-heme peroxidases mechanism of activation. In *Iron Metabolism: Inorganic and Regulatory Mechanisms*, G.C. Ferreira, J.J.G. Moura, and R. Franco, eds. (Weinheim: Wiley-VCH), pp 95–115.
- Navazza, J., and Saludjian, P. (1997). AMoRe: an automated molecular replacement program package. *Methods Enzymol.* 276, 581–594.
- Nicholls, A., Sharp, K., and Honig, B. (1991). Protein folding and association: insights from the interfacial and thermodynamic properties of hydrocarbons. *Proteins* 11, 281–296.
- Otwinowski, Z., and Minor, W. (1997). Processing of X-ray diffraction data collected in oscillation mode. *Methods Enzymol.* 276, 307–326.
- Page, C.C., Moser, C.C., Chen, X., and Dutton, P.L. (1999). Natural engineering principles of electron tunnelling in biological oxidation-reduction. *Nature* 402, 47–52.
- Pelletier, H., and Kraut, J. (1992). Crystal structure of a complex between electron transfer partners, cytochrome *c* peroxidase and cytochrome *c*. *Science* 258, 1748–1755.
- Pettigrew, G.W. (1991). The cytochrome *c* peroxidase of *Paracoccus denitrificans*. *Biochim. Biophys. Acta* 1058, 25–27.
- Pettigrew, G.W., and Moore, G.R. (1990). *Cytochromes c: Biological Aspects*. (Berlin: Springer-Verlag).
- Piontek, K., Glumoff, T., and Winterhalter, K. (1993). Low pH crystal structure of glycosylated lignin peroxidase from *Phanerochaete chrysosporium* at 2.5 Å resolution. *FEBS Lett.* 315, 119–124.
- Poulos, T.L., and Kraut, J. (1980). A hypothetical model of the cytochrome *c* peroxidase cytochrome *c* electron transfer complex. *J. Biol. Chem.* 255, 10322–10330.
- Poulos, T.L., Edwards, S.L., Wariishi, H., and Gold, M.H. (1993). Crystallographic refinement of lignin peroxidase at 2 Å. *J. Biol. Chem.* 268, 4429–4440.

Prazeres, S., Moura, J.J.G., Moura, I., Gilmour, R., Goodhew, C., Pettigrew, G.W., Ravi, N., and Huynh, B.H. (1995). Mössbauer characterization of *Paracoccus denitrificans* cytochrome c peroxidase. *J. Biol. Chem.* **41**, 24264–24269.

Reichardt, M., and Rogers, S. (1998). Preparation and analysis of DNA. In *Current Protocols in Molecular Biology*, F.M. Ausubel, R. Brent, and R.E. Kingston, eds. (New York: John Wiley & Sons).

Roussel, A., and Cambillau, C. (1989). TURBO-FRODO, molecular modeling package. In *Silicon Graphics Geometry Partner Directory*, Silicon Graphics, ed. (Mountain View, CA: Silicon Graphics) pp. 77–78.

Sambrook, J., Fritsch, E.F., and Maniatis, T. (1989). *Molecular Cloning: A Laboratory Manual, Second Edition* (Cold Spring Harbor, NY: Cold Spring Harbor Laboratory Press).

Shimizu, H., Schuller, D.J., Lanzilotta, W.N., Sundaramoorthy, M., Arciero, D.M., Hooper, A.B., and Poulos, T.L. (2001). Crystal structure of *Nitrosomonas europaea* cytochrome c peroxidase and the structural basis for ligand switching in bacterial di-heme peroxidases. *Biochemistry* **40**, 13483–13490.

Smet, L., Pettigrew, G.W., Guisez, Y., and Van Beeumen, J. (2001). Mutagenesis of the cytochrome c peroxidase from *Rhodobacter capsulatus*. *J. Inorg. Biochem.* **86**, 198.

Smith, A.T., and Veitch, N.C. (1998). Substrate binding and catalysis in heme peroxidases. *Curr. Opin. Chem. Biol.* **2**, 269–278.

Tezcan, F.A., Crane, B.R., Winkler, J.T., and Gray, H.B. (2001). Electron tunnelling in protein crystals. *Proc. Natl. Acad. Sci. USA* **98**, 5002–5006.

Tollin, G., Meyer, T.E., and Cusanovich, M.A. (1986). Elucidation of the factors which determine reaction-rate constants and biological specificity for electron-transfer proteins. *Biochim. Biophys. Acta* **853**, 29–41.

Weik, M., Raimond, B.G.R., Kryger, G., McSweeney, S., Raves, M.L., Harel, M., Gros, P., Silman, I., Kroon, J., and Sussman, J.L. (2000). Specific chemical and structural damage to proteins produced by synchrotron radiation. *Proc. Natl. Acad. Sci. USA* **97**, 623–628.

#### Accession Numbers

The coordinates (and structure factors) were deposited in the Protein Data Bank with the access codes 1RZ5 and 1RZ6 for forms OUT and IN respectively. The DNA sequence was deposited at the EMBL Nucleotide Sequence Database with the access code AJ630407.